Available online at www.sciencedirect.com
ScienceDirect
Journal of Solid State Chemistry 180 (2007) 3130–3135
JOURNAL OF SOLID STATE CHEMISTRY
www.elsevier.com/locate/jssc

Local atomic structure of a zirconia-based americium transmutation fuel

Marcus Walter[a,*], Catharina Nästren[a], Joseph Somers[a], Regis Jardin[a], Melissa A. Denecke[b], Boris Brendebach[b]

[a]European Commission, Joint Research Centre, Institute for Transuranium Elements, PO. Box 2340, D–76125 Karlsruhe, Germany
[b]Forschungszentrum Karlsruhe, Institut für Nukleare Entsorgung (INE), PO. Box 3640, D–76021 Karlsruhe, Germany

Received 3 July 2007; received in revised form 7 August 2007; accepted 12 August 2007
Available online 25 August 2007

Abstract

$(Zr,Y,Am)O_2$ with 6 and 19 mol% Am were prepared by infiltration of americium in porous yttria-stabilised zirconia (YSZ) beads. Samples were sintered at 1600 °C in Ar/H_2 to yield Am(III). By annealing them at 1000 °C in flowing air, the Am is oxidised to Am(IV). Both Am(III) and Am(IV) samples exhibit the presence of a single $(Zr,Y,Am)O_2$ phase with fluorite structure. The local atomic structure around the Zr, Y, and Am atoms is determined by EXAFS analysis. The Zr–O bond distance decreases from 2.15 to 2.12 Å with increasing Am(III) content, whereas the Y–O bond distance is independent of Am content and oxidation state. The Am(III)–O bond distance is 2.37 Å for both Am concentrations, while oxidation to Am(IV) decreases the Am(IV)–O distance to 2.28 Å, with a simultaneous expansion of the environment around the Zr atoms. The Am–O bond distances are contracted compared with the compounds $Am_2Zr_2O_7$ and AmO_2 and the distances expected from the ionic radii.

Keywords: Transmutation; Minor actinide; Americium; Zirconia; YSZ; EXAFS; Local structure

1. Introduction

The separation and transmutation of plutonium and minor actinides (MA = Np, Am, Cm) in nuclear reactors or accelerator-driven systems can reduce the long-term radiotoxicity of spent nuclear fuel. Inert (non-fertile) fuels are necessary as host matrices for the minor actinides to obtain a high MA transmutation efficiency. Zirconia-based compounds, either as yttria-stabilised zirconia (YSZ) or in a pyrochlore form, are considered as suitable inert matrices.

A novel process route for the fabrication of $(Zr,Y,MA)O_{2-x}$ fuel, which avoids generation of highly radioactive dust in the fabrication facility, is based on the infiltration of porous YSZ beads with actinide solution [1]. The porous YSZ beads are produced by gel-supported precipitation in a conventional laboratory. Following calcination, they are transferred into active cells and infiltrated by Am nitrate solution. After calcination and sintering, the product compound is a solid solution of the components, crystallising in the fluorite structure ($Fm\bar{3}m$). Depending on the thermal treatment conditions of Am oxides, Am can be obtained in the trivalent and tetravalent oxidation state. Since AmO_2 can release oxygen at temperatures higher than 1000 °C [2], $(Zr,Y,Am)O_{2-x}$ transmutation fuels are sintered in Ar/H_2 atmosphere to obtain predominantly trivalent Am.

YSZ doped with 10–40 mol% Ce and Pu shows a linear increase in the $Fm\bar{3}m$ lattice parameter with increasing Ce and Pu concentration [1]. However, X-ray diffraction yields the bulk structure information averaged over several unit cells and is less sensitive to the local atomic structure within the solid solution. Extended X-ray absorption fine structure (EXAFS) provides this complementary information for each type of metal atom in the $(Zr,Y,Am)O_{2-x}$ solid solution. In YSZ both the Zr (host) and Y (dopant) atoms

*Corresponding author. Fax: +49 7247 951 566.
E-mail addresses: marcus.walter@ec.europa.eu (M. Walter), joseph.somers@ec.europa.eu (J. Somers).

0022-4596/$ - see front matter © 2007 Elsevier Inc. All rights reserved.
doi:10.1016/j.jssc.2007.08.008

have a characteristic local environment, which differs from the bulk crystallographic structure. The Zr–O bond length in YSZ is generally shorter (2.14–2.17 Å) and the Y–O bond length is longer (2.28–2.32 Å) than the average value calculated from the bulk structure [3–5]. Beside investigations on YSZ containing both Ce and Er as dopant [6,7], most EXAFS studies on YSZ are associated with non-nuclear applications and no information on the local structure of YSZ containing minor actinides or Pu are available yet. The aim of the present study is to investigate the local atomic structure in an YSZ-based Am transmutation fuel $(Zr,Y,Am)O_2$ both for the trivalent and tetravalent Am oxidation state.

2. Experimental

2.1. Sample preparation

Two $(Zr,Y,Am)O_{2-x}$ samples with 6 and 19 mol% Am were prepared by infiltration of porous $(Zr_{0.84}Y_{0.16})O_{1.92}$ beads with Am nitrate solution. The YSZ beads were produced by a sol-gel process. This process involves dissolving zirconyl chloride and yttrium nitrate (both Alfa Aesar) in water and mixing them to give an yttrium concentration of 16 mol%, which is generally sufficient to obtain a final product with a cubic crystal structure. The viscosity of the starting solution was increased by adding polymer (Methocel, Dow Chemicals) [1,5]. The solution was then atomised and the droplets collected in an ammonia bath, where droplet-to-particle conversion is achieved. These particles were then washed in water and, following drying, they were calcined at 850 °C in air. During this step, the hydroxide precipitate is converted to oxide, and the polymers used in the process are removed by pyrolysis. The obtained calcined particles are highly porous, which makes them ideally suited for actinide infiltration.

Infiltration of the calcined beads with $Am(NO_3)_3$ solution was performed in the Minor Actinide Laboratory of the Institute for Transuranium Elements. The concentration of the Am solution was approximately 100 and 270 g/l for the low and high Am content samples, respectively. After drying, the beads were again calcined to remove nitrate ions and humidity. Sintering of the calcined beads was performed at 1600 °C in Ar/H_2 (8% H_2) for 6 h. Because of the reducing atmosphere the Am was predominantly in the trivalent oxidation state Am(III) in the product, as also indicated by its cinnabar red colour. After sintering, parts of both samples were annealed in air at 1000 °C for 24 h to oxidise Am to the predominantly tetravalent oxidation state Am(IV). During the oxidation the sample colour changes to greyish-black. In addition, $(Am_{0.2}Nd_{1.8})Zr_2O_7$ and AmO_2 compounds were prepared as XANES (X-ray absorption near edge structure) references for Am(III) and Am(IV), respectively.

X-ray diffraction measurements were performed using a Bruker D8 diffractometer ($CuK\alpha_1$, Ge monochromator) equipped with a position sensitive detector (PSD-50, M. Brown). The 2θ scanning range for all samples was from 20° to 120° with a 0.0085° step size. Lattice parameters for the $Fm\bar{3}m$ structure are obtained by refinement of the experimental diffraction pattern using Powdercell [8].

2.2. X-ray absorption measurement

The $(Zr,Y,Am)O_{2-x}$ and reference samples were milled, mixed with dried MgO to obtain an edge jump of approximately one for Zr, and pressed into discs for X-ray absorption measurement. The XAFS data at the Y and Zr K-edge and at the Am L_3-edge were recorded at the INE-Beamline at the Ångströmquelle Karlsruhe, ANKA [9]. A pair of Ge(422) crystals were used in the double-crystal monochromator, and two Rh-coated mirrors at this beamline ensure the rejection of higher harmonics. The photon energy of the light coming from the DCM was calibrated against the first maximum in the first derivative XANES spectrum of a Zr foil, defined as 17 998 eV. All measurements were performed at room temperature in transmission mode.

The EXAFS oscillations were extracted according to standard procedures (background removal by polynomial pre-edge fit, normalisation, cubic spline fit) using the EXAFSPAK program suite [10]. The threshold energy, E_0, was set to 17 055 eV for the Y K-edge, 18 010 eV for the Zr K-edge, and 18 520 eV for the Am L_3- edge. A spherical 8 Å cluster of atoms with Cartesian coordinates of the $Am_2Zr_2O_7$ pyrochlore ($Fd\bar{3}m$) structure [11] was used for the calculation of theoretical phase shifts, $\delta(k)$, and backscattering amplitude functions, $F(k)$ (FEFF8 [12]). Because of the similar backscattering properties, the same phase shifts and backscattering amplitude functions were used for Zr and Y. The amplitude reduction factor was held constant at 1.0 for the EXAFS fits. The shift in threshold energy, ΔE_0, was varied as a global parameter in the fit procedure.

3. Results

3.1. X-ray diffraction

The lattice parameter of $(Zr_{0.84}Y_{0.16})O_{1.92}$ increases with Am(III) doping from 5.142 Å (without Am), to 5.173 Å at 6 mol% Am(III), and 5.210 Å at 19 mol% Am(III). The diffraction peaks are significantly broader with increasing Am(III) content. Annealing the samples in air at 1000 °C leads to a decrease in lattice parameter to 5.164 Å for the 6 mol% Am(IV) sample and to 5.191 Å, for the 19 mol% Am(IV) sample.

3.2. Am L_3-edge XANES

The XANES spectra of $(Zr_{0.67}Y_{0.14}Am_{0.19})O_{2-x}$ in the oxidised and reduced state are shown in Fig. 1 together with those for the reference compounds $(Am_{0.2}Nd_{1.8})Zr_2O_7$

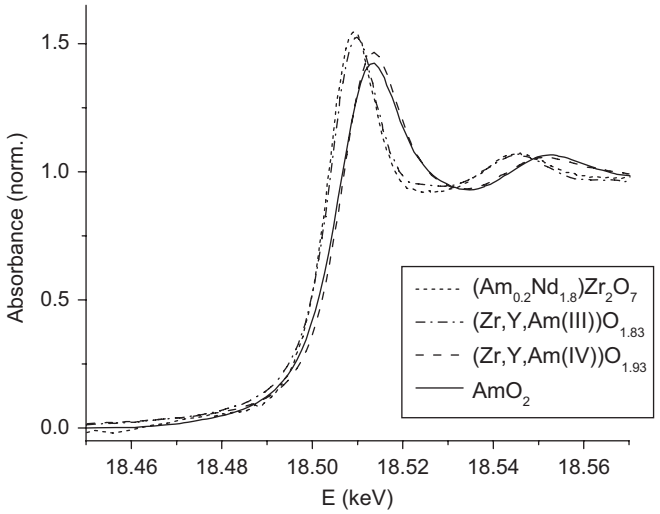

Fig. 1. Am L_3-edge XANES spectra of $(Am_{0.2}Nd_{1.8})Zr_2O_7$, AmO_2 and $(Zr_{0.67}Y_{0.14}Am_{0.19})O_{2-x}$ in the oxidised and reduced state. $(Am_{0.2}Nd_{1.8})Zr_2O_7$ and AmO_2 are reference compounds for Am in the trivalent and tetravalent oxidation state, respectively.

and AmO_2. The spectra of the samples with 6 (not shown) and 19 mol% Am are similar. The energy of the first maximum in the first derivate XANES for the reduced $(Zr,Y,Am)O_{2-x}$ samples are identical to the Am(III) reference; likewise the oxidised samples show the same edge energy as the Am(IV) reference spectrum. This confirms that Am(III) and Am(IV) oxidation states are reached by the respective thermal treatment procedures applied in sample preparation.

3.3. EXAFS

The k^3-weighted Zr, Y, Am EXAFS spectra of $(Zr_{0.67}Y_{0.14}Am(III)_{0.19})O_{1.83}$ and their Fourier transforms (FT) are shown in Fig. 2. The k-range of the EXAFS data is limited by element absorption edges at next higher energies, i.e., the Zr K-edge EXAFS range is limited by the Am L_3-edge and the Y K-edge is limited by the Np L_3-edge (traces of ^{237}Np are present as daughter of the ^{241}Am α-decay). In general, the EXAFS spectra are similar in shape and the corresponding FT's show two peaks in the 1.8 and 3.2 Å ($R+\Delta$) region. The first peak corresponds to the first coordination shell of approximately 8 oxygen atoms surrounding the Zr, Y and Am atoms. The second peak is due to 12 metal atoms in the second coordination shell, which can be Zr, Y, or Am. The amplitude of the first FT peak decreases with higher Am content for the Y and Am EXAFS spectra. The amplitude of the second peak exhibits no apparent trend for the three edges. In agreement with $(Zr,Y)O_{2-x}$ EXAFS data, no significant peaks are observed at higher distances [4].

The experimental EXAFS spectra were fitted using a two-shell model consisting of 8 O and 12 Zr atoms. The coordination number (N) of O atoms surrounding Zr was allowed to vary, since the trivalent atoms create oxygen vacancies which are mainly associated with Zr [4]. Americium is 8-fold coordinated in $Am_2Zr_2O_7$ and AmO_2 and consequently N(Am–O) was held constant. The backscattering behaviour of Zr and Y is similar (they are $Z+1$ elements), so that the Zr shell in the fit model represents both Zr and Y atoms. Compared with Zr or Y, Am has a very different backscattering phase shift and amplitude function. The resulting theoretical phase shift difference ΔR between the Zr–Zr and Zr–Am paths is about 0.25 Å, which allows simultaneous refinement of the Zr/Y and Am backscattering atoms. Therefore, the experimental data were also fitted using a three-shell model, in which the second coordination shell is modelled with Zr and Am subshells. Within the second shell, the sum of Zr/Y and Am atoms was held constant at the crystallographic value 12 and the ratio of the subshells was varied. As might be expected from its higher Am content, the 3-shell model gave better fit results for the 19 mol% Am samples. Confident structural parameters for the Am backscattering contribution in the 6 mol% Am samples could only be derived from the Zr K-edge EXAFS spectra. The structural parameters obtained from EXAFS analysis using these fit models are listed in Table 1 and an associated structural model is presented in Fig. 3.

3.4. Metal–oxygen coordination (nearest neighbours)

The bond length of the oxygen atoms surrounding Zr in $(Zr_{0.84}Y_{0.16})O_{1.92}$ is 2.15 Å. The same Zr–O distance is also observed in both oxidised $(Zr,Y,Am)O_{2-x}$ samples and in $(Zr_{0.78}Y_{0.16}Am(III)_{0.06})O_{1.89}$. In contrast, the Zr–O bond distance in $(Zr_{0.67}Y_{0.14}Am(III)_{0.19})O_{1.83}$ is 2.12 Å, i.e. significantly shorter than in the other samples. The number of oxygen atoms surrounding the Zr is approximately 6 and does not vary with the Am concentration or vary significantly with Am oxidation state. The Y–O bond length is 2.31 Å for $(Zr_{0.84}Y_{0.16})O_{1.92}$ and is in the range of 2.30–2.32 for Am doped samples. The coordination number of the Y–O shell (for the fits where it is allowed to vary) is close to the crystallographic value of 8. The Am–O bond length obtained differs for Am in the predominat trivalent state, compared with that in samples with predominantly tetravalent Am. The Am–O bond length is 2.37 Å for Am(III) and 2.28 Å for Am(IV) samples, and no dependence of the Am–O distance on the Am concentration can be observed.

3.5. Metal–metal coordination (next nearest neighbours)

In the $Fm\bar{3}m$ fluorite structure each metal atom is surrounded by 12 metal atoms (in this case Zr + Y + Am = 12) as next nearest neighbours. In undoped YSZ, the Zr–Zr/Y distance is 3.57 Å and the Y–Zr/Y distance is 3.60 Å. Doping YSZ with Am modifies the distances of this coordination shell and separate Zr–Am and Y–Am subshells can be distinguished. We observe that the distance between Zr/Y atoms and the central Zr atom

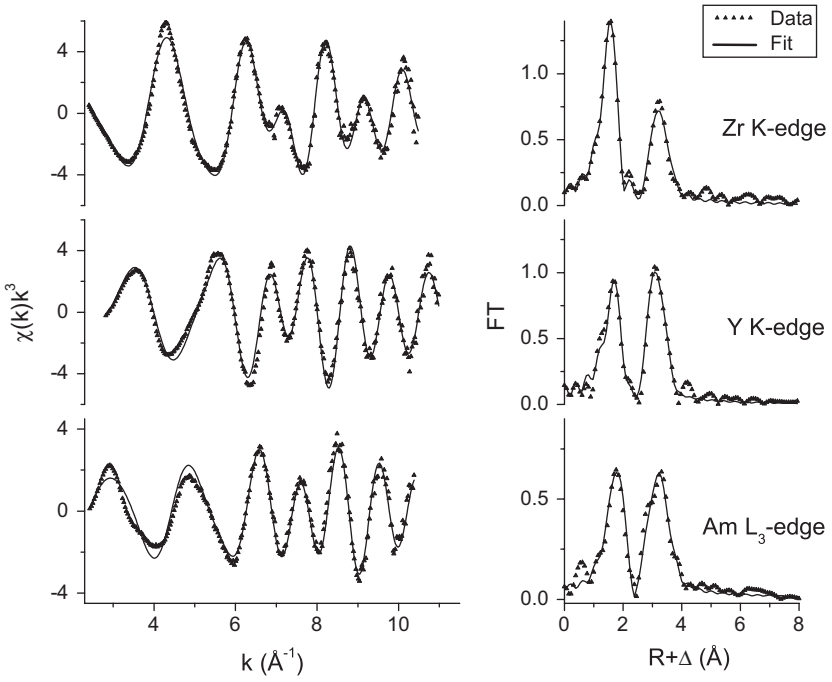

Fig. 2. Zr, Y K-edge and Am L_3-edge EXAFS spectra and FT of $(Zr_{0.67}Y_{0.14}Am(III)_{0.19})O_{1.83}$.

Table 1
Structural parameters for Zr,Y and Am in $(Zr,Y,Am)O_{2-x}$[a]

	N[b]	R (Å)[c]	σ^2 (Å^2)[d]	N	R (Å)	σ^2 (Å^2)
	$(Zr_{0.84}Y_{0.16})O_{1.92}$					
Zr–O	6.2 (2)	2.152 (2)	0.0084 (4)			
Zr–Y/Zr	12[f]	3.566 (2)	0.0108 (1)			
Y–O	8.4 (5)	2.311 (3)	0.0094 (6)			
Y–Y/Zr	12[f]	3.603 (2)	0.0073 (1)			
	$(Zr_{0.78}Y_{0.16}Am(III)_{0.06})O_{1.89}$			$(Zr_{0.78}Y_{0.16}Am(IV)_{0.06})O_{1.92}$		
Zr–O	6.0 (2)	2.149 (3)	0.0081 (4)	5.8 (2)	2.151 (3)	0.0083 (4)
Zr–Y/Zr	11.1 (9)	3.548 (4)	0.0137 (6)	11.3 (7)	3.569 (3)	0.0125 (5)
Zr–Am	0.9[e]	3.636 (7)	0.0038[f]	0.7[e]	3.630 (9)	0.0038[f]
Y–O	8[f]	2.316 (6)	0.0133 (6)	7.7 (4)	2.306 (2)	0.0089 (5)
Y–Y/Zr	12[f]	3.607 (5)	0.0082 (2)	12[f]	3.601 (2)	0.0084 (1)
Am–O	8[f]	2.375 (5)	0.0109 (4)	8[f]	2.272 (6)	0.0129 (6)
Am–Y/Zr	12[f]	3.615 (4)	0.0106 (2)	12[f]	3.618 (4)	0.0075 (2)
	$(Zr_{0.67}Y_{0.14}Am(III)_{0.19})O_{1.83}$			$(Zr_{0.67}Y_{0.14}Am(IV)_{0.19})O_{1.93}$		
Zr–O	6.5 (2)	2.123 (2)	0.0100 (3)	6.6 (2)	2.149 (2)	0.0083 (3)
Zr–Y/Zr	10.5 (11)	3.497 (3)	0.018 (1)	10.7 (11)	3.538 (3)	0.0152 (9)
Zr–Am	1.5[e]	3.624 (4)	0.0038 (3)	1.3[e]	3.646 (5)	0.0038 (5)
Y–O	8.2 (4)	2.297 (4)	0.0127 (6)	8.9 (6)	2.323 (6)	0.0130 (8)
Y–Y/Zr	9.5 (9)	3.594 (4)	0.0112 (7)	10 (1)	3.613 (5)	0.0091 (7)
Y–Am	2.5[e]	3.676 (7)	0.011 (1)	2[e]	3.74 (1)	0.008 (1)
Am–O	8[f]	2.367 (5)	0.0145 (3)	8[f]	2.292 (5)	0.0138 (3)
Am–Y/Zr	10(1)	3.620 (4)	0.013 (1)	9(1)	3.630 (4)	0.010 (1)
Am–Am	2[e]	3.713 (7)	0.007 (1)	3[e]	3.696 (6)	0.007 (1)

[a]Estimated standard deviations in parentheseis.
[b]N coordination number.
[c]R interatomic distance.
[d]σ^2 Debye–Waller factor.
[e]Sum of Y, Zr and Am atoms in the second coordination shell was held constat at 12.
[f]Parameter was fixed during the fit.

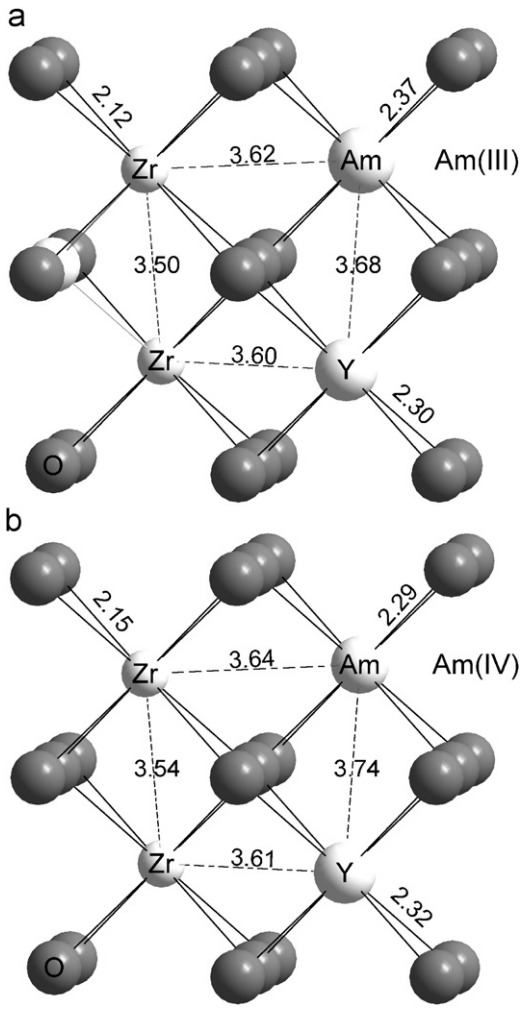

Fig. 3. Structural model of the $(Zr_{0.67}Y_{0.14}Am_{0.19})O_{2-x}$ local structure with Am as Am(III) (a) and Am(IV) (b).The oxidation of Am(III) to Am(IV) contracts the local Am–O bond lengths and relaxes the Zr environment.

in the Am(III)-doped samples decreases from 3.57 Å (YSZ), to 3.55 Å (6 mol% Am), and 3.50 Å (19 mol% Am). In contrast, there is no shortening for YSZ doped with 6 mol% Am(IV) (Zr–Zr/Y 3.57 Å), and only a 0.03 Å decrease for YSZ doped with 19 mol% Am(IV) (Zr–Zr/Y 3.54 Å). The disorder (σ^2) associated with this coordination shell increases significantly with the Am content of the samples. In addition to the Zr–Zr/Y subshell, Am atoms surrounding the Zr atoms are detected at distance of 3.62–3.65 Å. The obtained Debye–Waller factor ($\sigma^2 = 0.0038$ Å^2) were used for the fit of the 6 mol% Am samples to derive reasonable results. Despite the relatively high uncertainty associated with coordination numbers from EXAFS analysis, the obtained coordination numbers, N(Zr–Zr/Y) and N(Zr–Am), are close to that expected simply from stoichiometry consideration, excluding the formation of clusters enriched in Am.

In contrast to the Zr environment, the Y–Zr/Y distance is 3.60–3.61 Å, and is independent of the Am content and oxidation state. As for the Zr–Zr/Y distribution, the disorder (σ^2) increases with the Am content. The Y–Am distance derived from the subshell analysis for the samples with 19 mol% Am, is longer than for Zr–Am and is 3.68 and 3.74 Å for Am(III) and Am(IV), respectively. The disorder associated with this shell is similar to that observed for Y–Zr/Y, but higher compared to the Zr–Am distribution.

The distance between Zr/Y atoms surrounding the Am atoms (Am–Zr/Y) is 3.62–3.63 Å, and is independent of the Am oxidation state. This is essentially the same distance as that found for Am atoms surrounding Zr (Zr–Am). The largest difference between the Am–Zr/Y and Zr–Am distances is 0.021 Å. The disorder reflected in σ^2 values of the Am–Zr/Y shell increases with the Am content and is enhanced for the Am(III) samples, compared to their Am(IV) counterpart. For the samples with 19 mol% Am, the Am–Am distance is 3.70–3.71 Å with a similar disorder for both oxidation states.

4. Discussion

The compounds $Am_2Zr_2O_7$ and AmO_2 are suitable for comparison of determined interatomic distances. In $Am_2Zr_2O_7$, where Am is trivalent, the Am(III) ions are surrounded by 2 O atoms at 2.31 Å and 6 O atoms at 2.54 Å [11]. The average Am(III)–O bond length of 2.48 Å is similar to the bond length of 2.47 Å calculated from ionic radii [13]. The Zr atoms are coordinated by 6 O atoms at 2.12 Å. Compared with the fluorite structure, the oxygen vacancy in $Am_2Zr_2O_7$ is associated with the Zr atoms. The determined Am(III)–O bond distance of 2.37 Å in $(Zr,Y,Am)O_{2-x}$ is shorter than the 2.48 Å average in pyrochlore. Such a shortening of the Am(III)–O bond length compared with the pyrochlore structure is also found for large trivalent rare earth elements in stabilised zirconia [14].

For Am(IV), the Am–O bond length in the isostructural ($Fm\bar{3}m$) AmO_2 is 2.33 Å [15] and the same distance is determined from the ionic radii [13]. The Am(IV)–O bond length in the $(Zr,Y,Am)O_{2-x}$ measured in this investigation is 2.28 Å. i.e. shorter than in AmO_2. Compared with the reference compounds, the Am(III) environment in the YSZ inert matrix is more contracted than for Am(IV). The Am(III) ion is much larger than the Zr and Y ions and the resulting structural misfit is compensated by the observed contraction of the Am–O bond length. This structural misfit is lower for the smaller Am(IV) ion and the Am(IV)–O bond length derived by EXAFS analysis is closer to the distance expected from AmO_2 and the ionic radii.

The change of the Am oxidation state by annealing at 1000 °C in air mainly affects the coordination environment of Zr and Am, but not that of Y (see Fig. 3). The Am–O bond length decreases from 2.37 to 2.28 Å, which is correlated to a relaxation of the Zr environment, reflected in a significant increase in both the Zr–O and Zr–Zr/Y distances. This behaviour can be explained by the

stabilisation mechanism of cubic ZrO_2 by addition of dopant cations into the structure. Pure ZrO_2 is monoclinic at room temperature. By doping with larger, aliovalent cations such as Y(III) and Am(III), the cubic $Fm\bar{3}m$ structure can be stabilised at room temperature. The aliovalent doping creates oxygen vacancies associated with the Zr atoms and $^{[7]}$Zr polyhedra are formed, replacing some of the $^{[8]}$Zr. At low and intermediate concentrations Y remains 8-fold coordinated ($^{[8]}$Y) [4,16]. Doping with larger tetravalent ions such as Ce(IV) [17] also stabilises ZrO_2 in the tetragonal or cubic form. However, compared with the corresponding trivalent cations, the resulting solid solutions must contain much more Ce(IV) than, for example, Nd(III) to reach full cubic stabilisation [17]. Tetravalent substitution is isovalent and no oxygen vacancies are introduced and all Zr atoms stay in $^{[8]}$Zr coordination. The oxidation of (Zr,Y,Am(III))O_{2-x} shows a similar effect. As Am(III) is oxidised to Am(IV), the oxygen vacancies are filled and $^{[7]}$Zr becomes $^{[8]}$Zr, relaxing its local structure by stretching the Zr–O and Zr–Zr/Y distances. The presence of the cubic $Fm\bar{3}m$ structure of (Zr,Y,Am)O_{2-x} is preserved by the Y dopant, which does not change its valence.

5. Conclusion

The local atomic structure around Zr, Y and Am atoms in an YSZ based transmutation fuel was studied by EXAFS spectroscopy. The coordination environment of Zr contracts with increasing Am(III) content in (Zr,Y,Am)O_{2-x}. During oxidation the Am–O bond distance decreases from 2.37 to 2.28 Å and the Zr environment expands, indicating that the oxygen vacancies introduced by Am(III) are associated with the Zr polyhedra. The incorporation of Am(III) in YSZ lattice is accompanied by a contraction of the Am ions and EXAFS analysis of the next nearest neighbours indicates a homogeneous distribution of Zr, Y, and Am instead of a cluster formation.

Acknowledgments

We would like to acknowledge the assistance of A. Accarier, H. Hein, M. Holzhäuser and C. Boshoven in the preparation of samples, and thank the Ångströmquelle Karlsruhe, ANKA, for providing beamtime for the EXAFS measurements.

References

[1] A. Fernández, D. Haas, R.J. Konings, J. Somers, J. Am. Ceram. Soc. 85 (2002) 694.
[2] T.D. Chikalla, L. Eyring, J. Inorg. Nucl. Chem. 29 (1967) 2281.
[3] M.H. Tuilier, J. Dexpert-Ghys, H. Dexpert, P. Lagarde, J. Solid State Chem. 69 (1987) 153.
[4] P. Li, I.-W. Chen, J.E. Penner-Hahn, Phys. Rev. B 48 (1993) 10074.
[5] M. Walter, J. Somers, A. Fernandez, E.D. Specht, J.D. Hunn, P. Boulet, M.A. Denecke, C. Göbel, J. Mater. Sci. 42 (2007) 4650.
[6] C. Degueldre, S.D. Conradson, Appl. Phys. A 73 (2001) 489.
[7] P. Villella, S.D. Conradson, F.J. Espinosa-Faller, S.R. Foltyn, K.E. Sickafus, J.A. Valdez, Phys. Rev. B 64 (2001) 104101.
[8] W. Kraus, G. Nolze, J. Appl. Cryst. 29 (1996) 301.
[9] M.A. Denecke, J. Rothe, K. Dardenne, H. Blank, J. Hormes, Phys. Scr. T 115 (2005) 1001.
[10] G.N. George, I.J. Pickering, EXAFSPAK: A Suite of Computer Programs for Analysis of X-ray Absorption Spectra, Standford Synchrotron Radiation Laboratory, Stanford, 1995.
[11] R.C. Belin, P.J. Valenza, P.E. Raison, Structure of the americium pyrochlore $Am_2Zr_2O_7$ and its evolution under alpha self-irradiation, in: Proceedings of Actinides 2005, Manchester, 2005.
[12] A.L. Ankudinov, B. Ravel, J.J. Rehr, S.D. Conradson, Phys. Rev. B 58 (1998) 7565.
[13] R.D. Shannon, Acta Crystallogr. A 32 (1976) 751.
[14] D. Komyoji, A. Yoshiasa, T. Moriga, S. Emura, F. Kanamaru, K. Koto, Solid State Ionics 50 (1992) 291.
[15] D. Taylor, Br. Ceram. Trans. J. 83 (1984) 32.
[16] B.W. Veal, A.G. McKale, A.P. Paulikas, S.J. Rothman, L.J. Nowicki, Physica B 150 (1988) 234.
[17] H.M. Ondik, H.F. McMurdie (Eds.), Phase Diagrams for Zirconium and Zirconia Systems, The American Ceramic Society, Westerville, 1998.